Computer simulation of the CSPAD, ePix10k, and RayonixMX170HS X-ray detectors

Adrienne Tiña

Linac Coherent Light Source, Detectors Department at SLAC National Accelerator Laboratory
Science Undergraduate Laboratory Internship, U.S. Department of Energy

Abstract

The invention of free-electron lasers (FELs) has opened a door to an entirely new level of scientific research. The Linac Coherent Light Source (LCLS) at SLAC National Accelerator Laboratory is an X-ray FEL that houses several instruments, each with its own unique X-ray applications. This light source is revolutionary in that while its properties allow for a whole new range of scientific opportunities, it also poses numerous challenges. For example, the intensity of a focused X-ray beam is enough to damage a sample in one mere pulse; however, the pulse speed and extreme brightness of the source together are enough to obtain enough information about that sample, so that no further measurements are necessary. An important device in the radiation detection process, particularly for X-ray imaging, is the detector. The power of the LCLS X-rays has instigated a need for better performing detectors. The research conducted for this project consisted of the study of X-ray detectors to imitate their behaviors in a computer program. The analysis of the Rayonix MX170-HS, CSPAD, and ePix10k in particular helped to understand their properties. This program simulated the interaction of X-ray photons with these detectors to discern the patterns of their responses. A scientist's selection process of a detector for a specific experiment is simplified from the characterization of the detectors in the program.

I. Introduction

The X-ray has proven its worth and development since its discovery by Wilhelm Röntgen in 1895. Aside from its evident value in medicine, the X-ray has an unlimited number of possible contributions to scientific research. Free-electron lasers (FELs) produce radiation, e.g. X-rays, that can be harnessed to conduct all sorts of experimentation. SLAC National Accelerator Laboratory houses an X-ray FEL (XFEL) at its LCLS facility. An FEL can accelerate electrons to 99.999% of the speed of light by passing an electron beam through an undulator. The LCLS Undulator hall, comprised of thousands of alternating magnets, causes electrons to "wiggle" along a sinusoidal path. As the electron bunches travel, they interact with each other and emit radiation. The X-rays line up in phase (hence the "coherent" in LCLS), making them more powerful than those generated by previous light sources. Both SLAC employees and outside researchers from around the world conduct experiments in the various LCLS experimental hutches. Some examples include the Soft X-ray Research, Coherent X-ray Imaging, and the Matter in Extreme Conditions hutches (Descriptions of all hutches: White *et al* 2015). The advantage the LCLS offers is its capability to produce images and even movies of miniscule objects like molecules or atoms due to its properties. This light source does not come without its challenges, however. With such a fast repetition rate of 120 Hz, short pulses from ~30-200 fs, and extreme peak brightness (more than 10^9 times brighter than

This material is based upon work supported by the U.S. Department of Energy, Office of Science, Office of Workforce Development for Teachers and Scientists (WDTS) under the Science Undergraduate Laboratory Internship (SULI) program, under Contract No. DE-AC02-76SF00515.

previous sources), the radiation in its extremity has the capability of damaging a sample in a single pulse (figure 1). SLAC needs compatible X-ray imaging devices for use with LCLS to produce these aforementioned movies.

The extremity of the LCLS XFEL has proven to be a challenge for existing imaging instrumentation at SLAC: X-ray CCDs (charge-coupled devices). In recent years X-ray CCDs have provided the desired intensity information of the pulses with fairly good energy resolution. These CCDs are commonly used at synchrotrons, but their readout rates are not fast enough to match the repetition rate at LCLS (Blaj *et al* 2015). Two X-ray CCD detectors with low noise and good efficiency over a large energy range have been used at LCLS in different imaging and spectroscopy applications: the pnCCD (based on a pn-junction CCD sensor designed at the Halbleiterlabor in Germany) and fCCD (based on a MOS CCD sensor designed at the Lawrence Berkeley National Laboratory) (Blaj *et al* 2015). The pnCCD in particular has the outstanding properties of high quantum efficiency in the X-ray range, energy resolution, and high frame rate capability (Scharf *et* al 2011). While these two detectors are sufficient enough for use at LCLS, newer detectors with higher maximum signal would provide better capabilities in experimentation. In other words, more compatible detectors would allow scientists to take full advantage of the coherent light source and the types of scientific research it enables (figure 2). This work discusses a computer program that simulates three X-ray detectors – Rayonix MX170-HS, CSPAD, and ePix10k – that are all well suited contenders for possible use. The chosen are three of the small number of X-ray detectors at SLAC. The goal of the project to be discussed is that their behavior under different circumstances might be understood without the need for actual deployment.

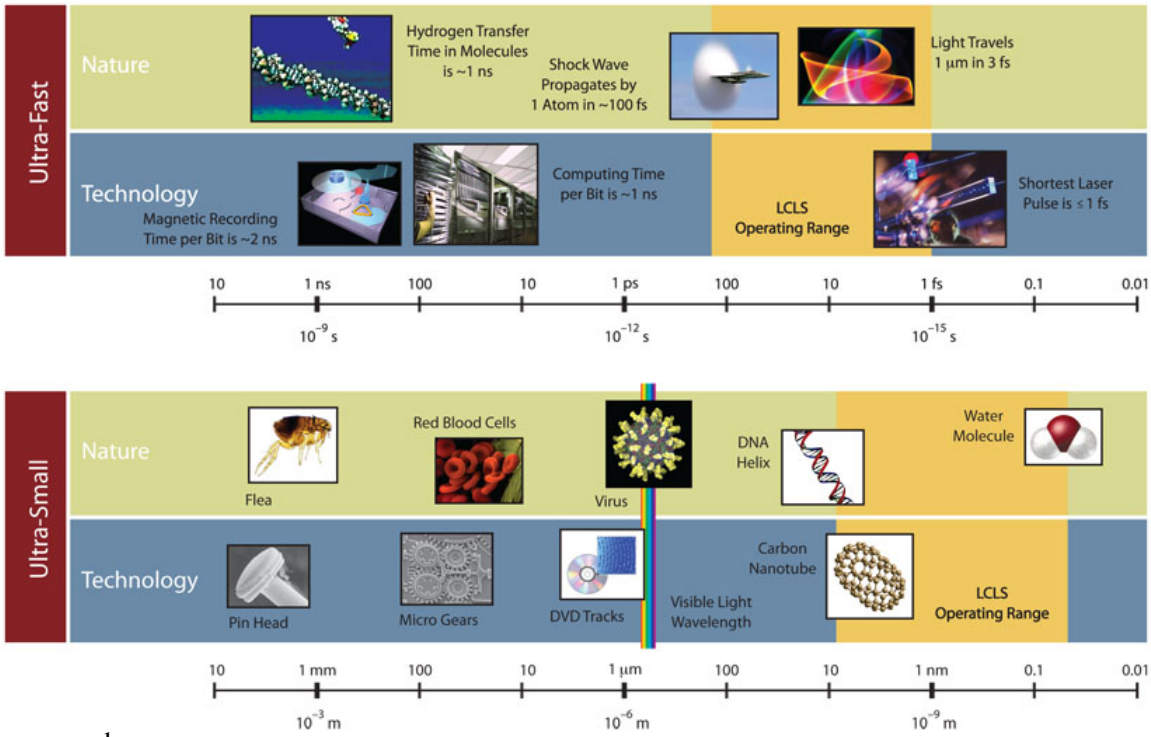

Figure 1.[1] Properties of the LCLS capabilities.

[1] SLAC National Accelerator Laboratory 2015.

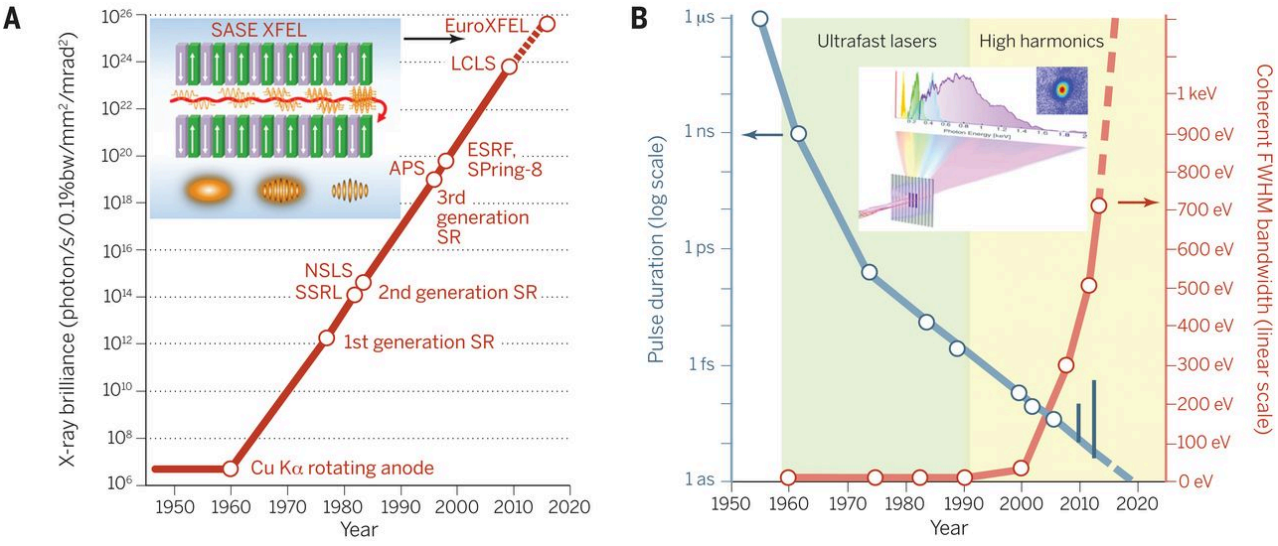

Figure 2.[2] (A) The X-ray brilliance of coherent light sources has improved by 20 orders of magnitude in 6 decades (brilliance is a measure of coherent X-ray flux). (B) Progress in tabletop coherent bandwidth and pulse duration as a function of year.

2. Instruments and Methods

2.1 Indirect Detector: Rayonix MX170-HS

The Rayonix MX170-HS (figure 3) is a member of the MX series of detectors manufactured by Rayonix, L.L.C. These CCD X-ray detectors, specifically designed for crystallography, are the only large format mosaic X-ray detectors without gaps in their imaging areas (Rayonix "About," 2015). The Rayonix MX170-HS is "indirect" due to the multi-step process it uses in radiation detection. Generally, the X-ray photons are absorbed by a scintillator, which converts these photons into visible light[3] (more information about the scintillation conversion mechanism can be found in Martin Nikl's publication, as cited in References). This visible light is then coupled to a CCD by a fiber optic plate (FOP). The FOP, comprised of μm-sized optical fibers, focuses the visible light for the CCD to process. Its main purpose is to protect the CCD from damaging, high-energy X-ray radiation. The light in the CCD is converted into electrons and collected into the pixels. These electrons are shifted into an output register via a binning technique[4] and converted into digital signals for further processing. The number of electrons that are required to form a single ADU (analog-to-digital unit) is specific to the detector's properties in its gain settings (Larsson 2013). After exposure, the digital signals provided by the CCD are what the computer would need to generate an image.

The advantages indirect detectors provide include large active area and fast readout speed. Large active area is highly desirable, as it gives scientists the capability to detect more information about a sample. Fast readout enables quick data processing. With

[2] Miao *et al* 2015.
[3] Scintillators could also fluoresce ultraviolet light, but this project assumes visible light.
[4] Binning is the process of combining charge from adjacent pixels in a CCD during readout. It is performed prior to digitization to speed up the readout process.

the rapid repetition rate and high pulse rate of the LCLS, these traits are extremely beneficial. Some costs of indirect detection include the inability to allow single photon counting (not so much an issue for LCLS) and very poor energy resolution (Carini 2012).

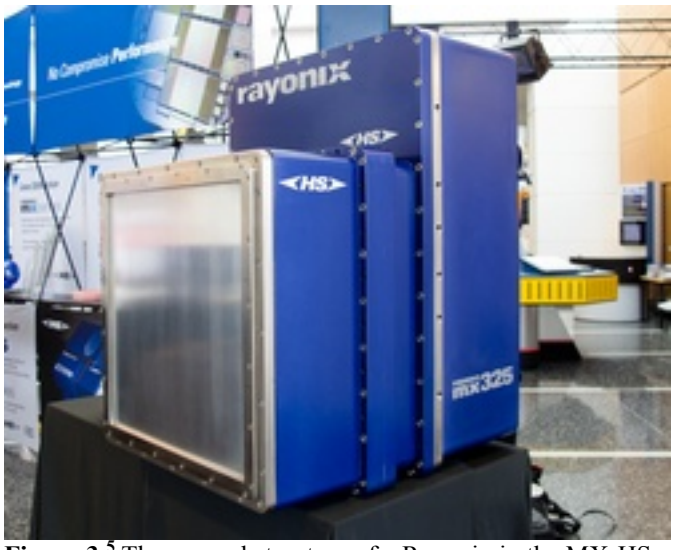

Figure 3.[5] The general structure of a Rayonix in the MX-HS series.

2.2 Direct Detectors: CSPAD and ePix10k

The direct detector essentially produces the same information provided by an indirect detector to form an image, but by a different process. Its name ensues the fact that the incident X-ray photons produce electrical signals by "directly" interacting with the semiconductor sensor pad (Carini 2012). The direct conversion detector simply uses a photoeffect in its sensor (typically silicon) to detect those X-rays and produce the signals (Herrmann 2013).

The CSPAD and ePix10k (figures 4 and 5) were both specifically developed for use at LCLS. The CSPAD, or Cornell-SLAC Pixel Array Detector, was a collaborative effort between Cornell University and SLAC National Accelerator Laboratory. A unique feature of its geometry is its ability to be arranged in multiple configurations. The tiles of its sensor pad could be arranged into the preferred form, depending on the area of expected photon activity in the experiment (Carini 2013). The ePix10k is a member of the ePix family of detectors. The ePix10k was specifically designed to replace the CSPAD for most hard X-ray experiments as it provides 10% better position resolution, nearly one-third lower noise, and four times higher dynamic range (Blaj *et al* 2015).

The advantages of a direct detector include good signal-to-noise ratios (excellent quantum efficiency and energy resolution), fast readout (ns charge collection time and high frame rates) and ability for use with pulsed sources with large instantaneous photon rates (Carini 2012, 2014).

[5] Rayonix "MX-HS…" 2015.

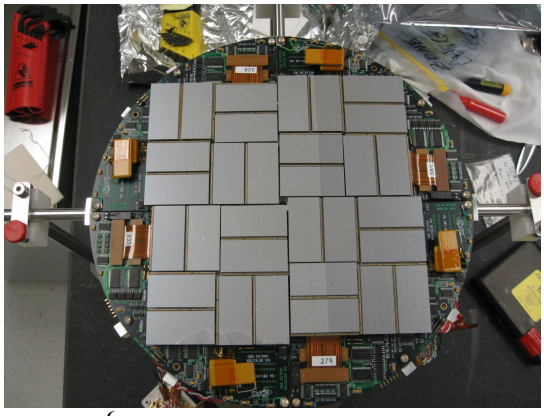

Figure 4.[6] (left) CSPAD in general configuration.
Figure 5.[7] (right) ePix camera. This is the assembly used for the different ePix detectors.

2.3 Design considerations

Numerous factors go into the configuration of a detector's design, all of which affect its functionality. These factors also affect the selection of a detector for experimentation. Some of these factors include:

1. Detector geometry[8]
2. Efficiency
3. Event rate
4. Readout rate
5. Cost

Although these factors are all equally significant, they cannot be optimized simultaneously. Generally, detectors are modified and optimized for use at different energy levels and usually provide some sort of tradeoff between high resolution and low noise rates, so it is key to choose the right detector for the right situation (Larsson 2013). The impact and importance of these factors are described in Spieler's publication cited under References. In any case, the X-ray detector is what limits the capabilities of the experiment, and although X-ray detectors have improved significantly in recent years, their improvement has not developed as significantly as the X-ray sources themselves (Gruner 2012).

2.4 Computer Simulation

The computer program began with a general detector class. Then three subclasses were made, representing each detector with its own settings and features. This allowed for the program to distinguish between the different detectors. Each detector class contained a number of tiles, which together, create a plane representing the detector's sensor pad. Where this plane resided in space represented how far one placed the detector from where the X-ray photons came.

[6] Dubrovin 2015.
[7] Blaj *et al* 2015.
[8] For more information, refer to Blaj's article containing tables with features of CSPAD and ePix10k.

Depending on the distribution and intensity of photons specified by the user of the program, a list of X-ray photons were generated, represented by vectors moving outward in space. The program calculated the intersections (if any) between these photon vectors; the detector stored that information within each pixel of its tiles. Each photon carried a cloud of charge, so the charge deposited in each pixel was spread out to the surrounding pixels. The charge was then converted into the corresponding number of ADUs, as specified by the gain setting of the detector.[9] Noise was then applied to the camera. For the program's general purpose, the detectors' measured noise r.m.s. values were used. Finally, the ADUs were converted back into photons. These numbers were slightly different than the original counts, as charge had been spread and noise applied.

The concentration of photons-per-pixel and noise values combined represent the data needed for the computer to construct an image of the sample*.

3. Results

3.1 Indirect Detector: Rayonix MX170-HS

After the computer completed processing, a graph was produced. This graph displayed the intensity of photons by the average number of photons distributed in the detector's pixels. Figure 6 shows the graphs from two separate simulations of the Rayonix. Both simulations were run under the same conditions, with the only differing factor being the placement of the Rayonix in space. For this particular example, the distribution of photons was quadratic, the start intensity was 100,000, and the detector was placed at 10 a.u. (left) and 100 a.u. (right). The intensity of photons was incremented by 1,000 each run for 10 iterations, as shown on the x-axis of both graphs in Figure 6.

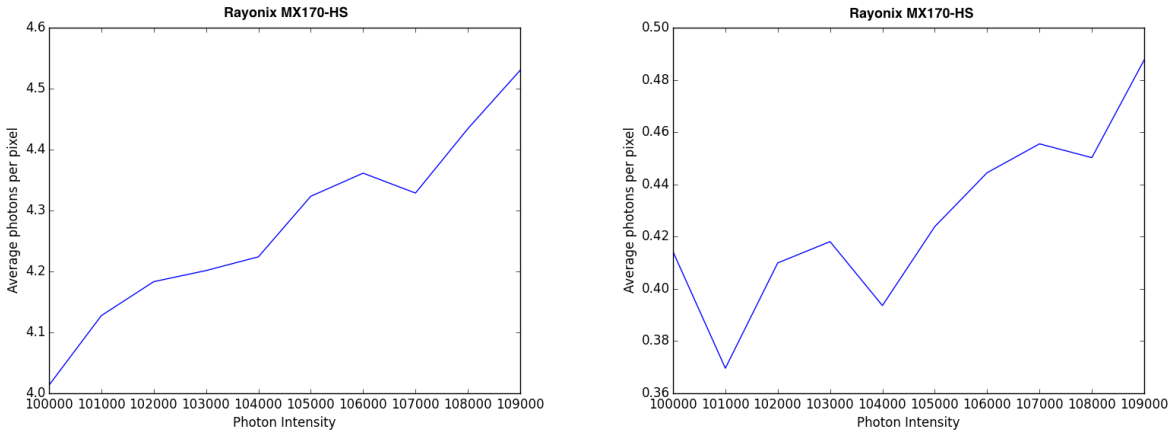

Figure 6. (a) (left) Rayonix with quadratic distribution, 100,000 start photon-intensity, 10 a.u. placement. (b) (right) Rayonix with quadratic distribution, 100,000 start photon-intensity, 100 a.u. placement.

[9] Gain on a detector represents the conversion factor between electrons into digital counts, or ADUs. Gain is represented as electrons per ADU (e^-/ADU).

* For a more detailed description of the computer code, see the Appendix section.

For a smoother graph and better visualization of the linear behavior, the number of iterations along the x-axis (photon intensity) was increased to 50 (figure 7). The intensity incrementation between iterations remained at 1,000 photons.

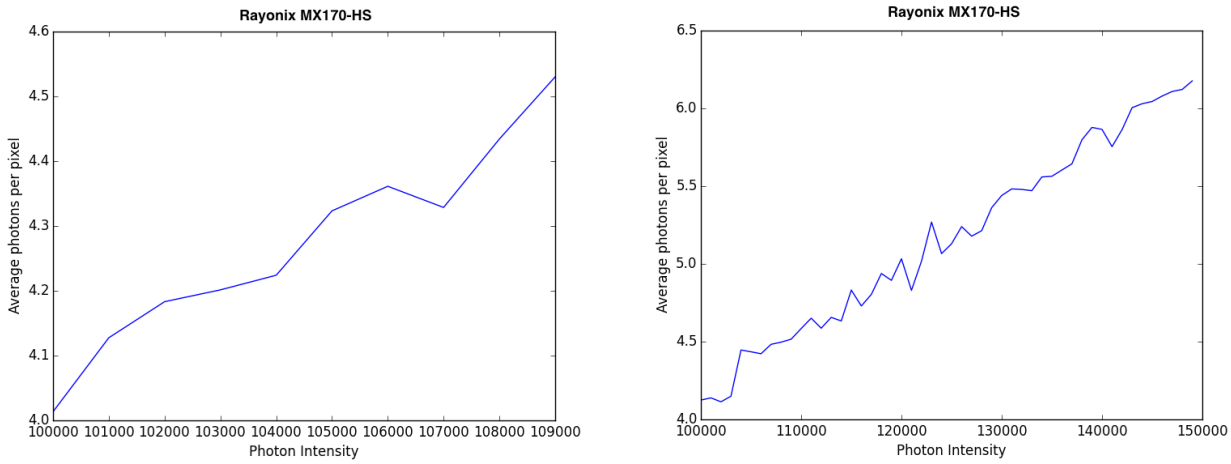

Figure 7. (a) (left) Repeat of Figure 6a: Rayonix with quadratic distribution, 100,000 photon-intensity, 10 a.u. placement, 10 iterations. (b) (right) Rayonix with quadratic distribution, 100,000 photon-intensity, 10 a.u. placement, 50 iterations.

3.2 Direct Detectors: CSPAD and ePix10k

The same simulation format was run for the CSPAD. Figure 8 displays the results of two CSPAD simulations: both ran under 100,000 start photon-intensity conditions and quadratic distribution, while the difference was in the positioning of the detector. As observed above in Figure 7, with increased number of iterations, a deeper understanding of patterns in the results could be seen. Hence, the correction was made, and the number of iterations for any graph from this point forward is now 50.

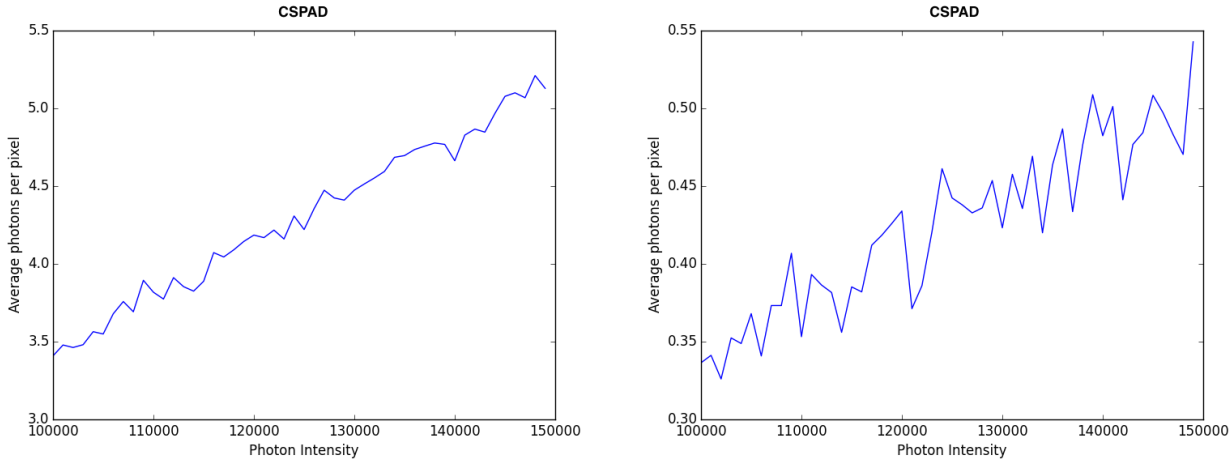

Figure 8. (a) (left) CSPAD with quadratic distribution, 100,000 start intensity, 10 a.u. placement. (b) (right) CSPAD with quadratic distribution, 100,000 start intensity, 100 a.u. placement.

Third, simulations of the ePix10k were performed under the same conditions as indicated above. The same linear pattern found in the Rayonix MX170-HS and CSPAD simulation graphical results were also discovered in the ePix10k. The linear behavior was expected, as it makes sense logically. Generally, if we increase the number of photons that are generated and keep our detector at the same point in space, then the behavior in number of intersected photons should be proportional to that increased intensity. The results of the ePix10k simulations can be seen in Figure 9 below.

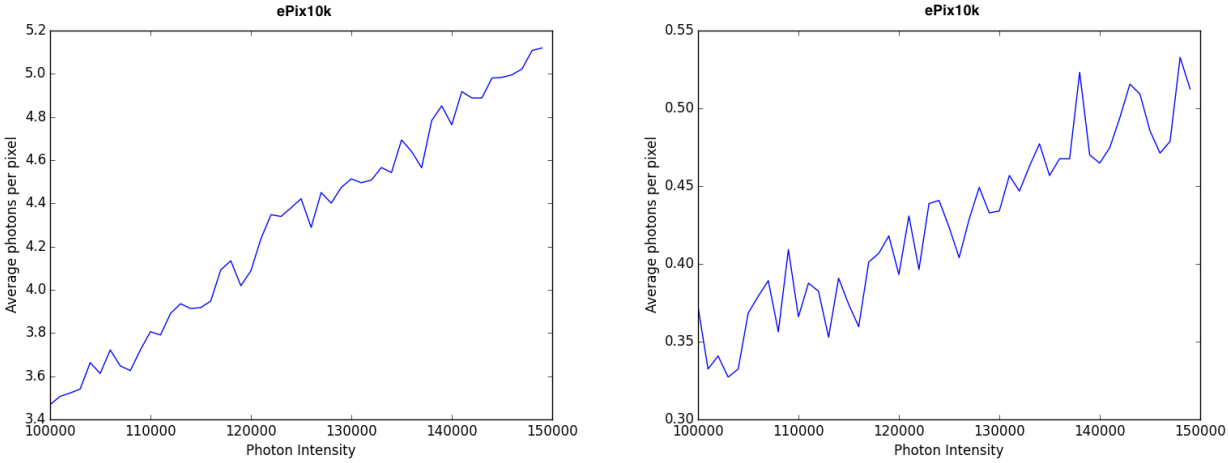

Figure 9. (a) (left) ePix10k simulation with quadratic distribution, 100,000 start intensity, 10 a.u. placement. (b) (right) ePix10k with quadratic distribution, 100,000 start intensity, 100 a.u. placement.

For all intensive purposes, the effects of changing the photon distribution type are not shown in this paper; however, upon testing these effects, the general conclusion was that with increased complexity of the distribution order – uniform, to linear, to quadratic, to fourth – the average number of intercepted photons increased accordingly. All simulations described in this paper are all quadratic.

4. Discussions and Conclusion

Under the same experimental settings, the three detectors behaved differently on a noticeable scale. The graphs produced by the computer simulation showed extremely comparable results. The Rayonix MX170-HS, when placed at 10 a.u. under fifty iterations of photon intensity levels, displayed exceptionally linear behavior in average photon-per-pixel counts (figure 7b). At 100,000 photons, the average number of photons per pixel absorbed by the detector was about 4.1 photons; however, in figure 7a, it is clear that at 100,000 generated photons, the actual number of photons per pixel is closer to 4 than it is to 4.1. Therefore, for better predictions of the general behavior of the detector, simulations with more iterations would be helpful; on the other hand, for more accurate readings of exact numerical values for photon averages, setting a smaller range of iterations would be ideal.

While the average number of photons per pixel in the Rayonix (figure 7b) ranged from 4.1 to roughly 6.2, the average range for the CSPAD at the same 10 a.u. distance was slightly lower, from about 3.5 to 5.1 (figure 8a). This means on average that the Rayonix absorbed nearly one more photon-per-pixel than the CSPAD. To refer back to its

advantages, the indirect detector has a large active area; hence the fact that the Rayonix had larger averages than the CSPAD. The same concept applies to the ePix10k, whose averages at 10 a.u. were lower than both the Rayonix and the CSPAD.

Upon analysis of the 100 a.u. graphs (figures 6b, 8b, 9b), we notice that although their photon intensity ranges mirror those of their 10 a.u. counterparts (figures 6a, 8a, 9a) from 100,000 to 150,000, their averages are all much lower. The average photon-per-pixel ranges were: Rayonix – 0.37-0.49; CSPAD – 0.33-0.55; ePix10k – 0.325-0.54. Since the detectors for these three simulations were placed much farther than 10 a.u., in theory the average number of photons they intercept should be lower. Based on these graphs, the simulation did demonstrate the expected behavior. For future optimization, error bars should be included in these graphs.

With the exponential development of science, the need for new compatible instrumentation is essentially interminable. In fields like cancer research, it is important that the least bit of restrictions are imposed, so to conduct the most advanced, groundbreaking research that the world so desperately desires and needs; therefore, having attuned devices that would help conduct these experiments is crucial. The model this project followed is the backbone to any form of experimentation: testing. Without device testing and characterization, choosing the proper equipment for a situation to obtain the most advanced information would not be possible.

In conclusion, this project helped to characterize the LCLS detectors by simulating their behavior. The program helped to understand how they work, what they output at certain settings, and their costs and benefits. Most importantly, the program will help a scientist determine which detector is most useful for a specific experiment. Generally, there is no better detector than another. It truly depends on the type of detector needed for the experiment being conducted. With the rapid pace of scientific development, instrumentation will continue to develop; the hope is that this program can be modified for future use, possibly for the coming of LCLS II!

Acknowledgements

This work is a result of the SULI program, funded by the U.S. Department of Energy. The project was completed under the mentorship of Gabriella Carini and Philip Hart. Special thanks to Enrique Cuellar and Maria Mastrokyriakos for their efforts.

Appendix

My program creates an abstract “Detector” class that holds variables representing the basic characteristics of SLAC’s detectors. These characteristics include the number of tiles that the detectors contain, pixel size, and frame readout rate. Subclasses, derived from the detector and indirect detector parent classes, represent the specific X-ray detectors used at SLAC. The features of each detector are specified within the subclasses.

The key attribute of the detector class is the “tiles” list. This list contains the equivalent number of tiles specified by the detector type, and each tile index in this list is its own separate “Tile” class. The “Tile” class contains the (x, y, z) coordinates of the tile, and the number of rows and columns of pixels per tile. The Detector class also contains a list of p-vectors that point to the position of each tile (tile coordinates), slow and fast-scan

vector arrays that define single pixels, a list of shape vectors which define the grid dimensions, and a list of normal vectors that help define the plane of the corresponding tile at a specific index. Purposefully, the index of every vector in each of these lists corresponds with the specific tile to which it belongs in the tiles list.

An OptionParser (optparse) interface is utilized for this program. Default settings are used if the user makes no specifications. Otherwise, the user has the option to select the specific detector to simulate, the desired order of the photon distribution, the start photon intensity, whether or not to utilize a pre-defined library of noise values, and the position of the detector in space.

At the instance the creation of a detector is prompted, the "tiles" list is created. This is done from one point coordinate, which represents the first tile. From there, the remaining correct number of tiles are created and placed accordingly in space to form a grid, depending on the coordinate of the first tile. With the tile grid ready, the correct normal, slow and fast-scan vectors are computed, which are used to detect possible intersections between the X-ray photons and the detector.

Next, the actual photon simulation begins. A list of photons are generated according to the distribution and intensity specified (the distribution is of the fourth order and intensity is 100,000 by default). The photon list is an array of 4-vectors in the form [a, b, c, E], where a, b, and c represent the direction in which the photon travels, and E represents its energy value. The program then sends this list of photons into a function entitled "findIntersections."

FindIntersections goes through the detector's list of tiles, and passes each individual tile index into the "calculate_intersect" function. This function computes the points where the photon vectors intersect the detector, via a series of dot product computations, array transposes, and assertions (to ensure viable data). Calculate_intersect returns two arrays: the first is an array containing the coefficients of the position of each intersection in terms of the tile's slow/fast-scan vectors (pixel locations), and the second is a Boolean array specifying if there is an intersection at each pixel. All of this information is gathered together to create a data array for each tile. If an intersection occurred at a pixel in the tile, then the "hit" count is stored into the data array at that location. Otherwise, the data value remains at zero.

The data array reflects the interaction of the X-ray beams and the detector sensor pad. After this information is stored, the charge of each photon is spread into the surrounding pixels. The charge is then converted into ADUs, with the detector-specific conversion unit determined by the gain setting (gain = e^-/ADU). If a pixel reaches full-well capacity (maximum charge pixel can hold), saturation occurs. This is represented by setting the charge in that pixel to its maximum, even if the total charge exceeds that value. Random noise values are then added to each pixel in the detector. These values are determined by the detectors' pre-determined noise r.m.s. values. After noise has been added, ADUs are converted back to photons. This number differs slightly from the initial photon count due to the charge deposited into surrounding pixels and added noise.

The average number of photons per pixel is recorded in each tile and totaled for that detector. As several iterations are run in the program, each with different photon intensities, the recorded average of each iteration is stored into a list. The graphs produced by the program plot the intensity of photons by each average number of photons per pixel stored in that list.

References

Blaj G., Caragiulo P., Carini G., Carron S., Dragone A., Freytag D., Haller G., Hart P., Hasi J., Herbst R., Herrmann S., Kenney C., Markovic B., Nishimura K., Osier S., Pines J., Reese B., Segal J., Tomada A., and Weaver M, "X-ray detectors at the LCLS," *Journal of Synchrotron Radiation*, 22(3) 577-83 (2015).

Carini G., Lecture SLAC National Accelerator Laboratory, "CSPADs: how to operate them, which performance to expect and what kind of features are available" (2013).

Carini G., Lecture SLAC National Accelerator Laboratory, "X-ray detectors for new photon science facilities: are they the remaining experimental limitation?" (2014).

Carini G., Lecture SLAC National Accelerator Laboratory, "Overview of Detectors for X-rays from 20-100 keV Area detectors" (2012).

Dubrovin, M., "LCLS: CSPAD Geometry and Alignment," SLAC National Accelerator Laboratory,https://confluence.slac.stanford.edu/display/PSDM/CSPAD+Geometry+and+Alignment#CSPADGeometryandAlignment-Detectorgeometrymodel (2015).

Gruner S. M., "X-Ray imaging detectors," *Physics Today*, 65(12) 29-34 (2012).

Herrmann S., Lecture SLAC National Accelerator Laboratory, "How a detector works?" (2013).

Larsson J., 2013: X-ray detector characterization – a comparison of scintillators, [Stockholm, Sweden]: Royal Institute of Technology.

Miao J., Ishikawa T., Robinson I. K., Murnane M. M., "Beyond crystallography: Diffractive imaging using coherent x-ray light sources," *Science Magazine*, 348(6234) 530-5 (2015).

Nikl M., "Scintillation detectors for x-rays," *Measurement Science and Technology*, 17(4) R37-54 (2006).

Rayonix, L.L.C., "About," http://www.rayonix.com/about/ (2015).

Rayonix, L.L.C., "MX-HS Series," http://rayonix.com/products/mx-hs-series/ (2015).

Scharf O., Ihle S., Ordavo I., Arkadiev V., Bjeoumikhov A., Bjeoumikhova S., Buzanich G., Gubzhokov R., Günther A., Hartmann R., Kühbacher M., Lang M., Langhoff N., Liebel A., Radtke M., Reinholz U., Riesemeier H., Soltau H., Strüder L., Thünemann A.F., and Wedell R., "Compact pnCCD-Based X-ray camera with high spatial and energy resolution: a color x-ray camera," *Journal of the American Chemical Society*, 83(7) 2532–8 (2011).

SLAC National Accelerator Laboratory, "Linac Coherent Light Source: About LCLS," https://portal.slac.stanford.edu/sites/lcls_public/aboutlcls/Pages/About-LCLS.aspx (2015).

Spieler H. (Lawrence Berkeley National Laboratory), in *Semiconductor Detector Systems*, edited by Nicholas R.J. and Kamimura, H. (Universities of Oxford and Tokyo, 2005), pp. 316-8.

White W. E., Robert A., and Dunne M., "The Linac Coherent Light Source," *Journal of Synchrotron Radiation*, 22(3) 472-6 (2015).